

# Multipactor Modeling in Cylindrical Dielectric-Loaded Accelerators

John G. Power\* and Steven H. Gold†

\* *High Energy Physics Division, Argonne National Laboratory, Argonne, IL 60439*

† *Plasma Physics Division, Naval Research Laboratory, Washington DC 20375*

**Abstract.** The observation of strong multipactor loading of a cylindrical dielectric-loaded accelerator (DLA) structure with an alumina liner was previously reported [1]. Conventional multipactor loading of dielectric rf windows is due to a tangential rf electric field and generally saturates at a few percent power loss. However, this resonant single-surface multipactor is driven by a combination of normal and tangential rf electric fields, is a strong function of the incident power, and is capable of absorbing a large fraction (over 1/2) of the incident rf power. Since the initial report, several additional structures have been tested, fabricated from a variety of materials, some with low secondary-emission surface coatings, and having different physical dimensions. In this paper, we summarize the results of these tests and analyze the results in terms of a physical model of the multipactor phenomenon.

**Keywords:** multipactor, linear accelerator, dielectric accelerator

**PACS:** 29.17.+w, 41.75.Lx, 52.80.Pi, 84.90.+a

## INTRODUCTION

In recent years, much effort has been devoted to developing new types of high gradient accelerating structures with gradients  $>100$  MV/m. One of the most promising of these technologies is the dielectric-loaded accelerating (DLA) structure (Fig. 1), where a cylindrical copper tube is lined with a dielectric sleeve (inner radius  $a$  and outer radius  $b$ ) and driven by an external RF source. A program is under way to test externally driven DLA structures at high gradients, and to develop a compact DLA test accelerator [2]. The structures are developed at Argonne National Laboratory (ANL) and tested at the Naval Research Laboratory (NRL). This paper presents results from recent high power tests of DLA structures.

The initial test of an alumina DLA structure showed strong multipactor loading [1]. Conventional multipactor loading of dielectric rf windows is due to a tangential rf electric field and generally saturates at a few percent power loss. However, this resonant single-surface multipactor is driven by a combination of normal and tangential rf electric fields, is a strong function of the incident power, and is capable of absorbing a large fraction (over 1/2) of the incident rf power. The power loss is accompanied by light emission from the inner surface of the dielectric. We developed a simple 2D cylindrically symmetric model that demonstrated the essential features of the experimental observations in the alumina DLA high power test.

CP877, *Advanced Accelerator Concepts: 12<sup>th</sup> Workshop*,  
edited by M. Conde and C. Eyberger

© 2006 American Institute of Physics 978-0-7354-0378-9/06/\$23.00

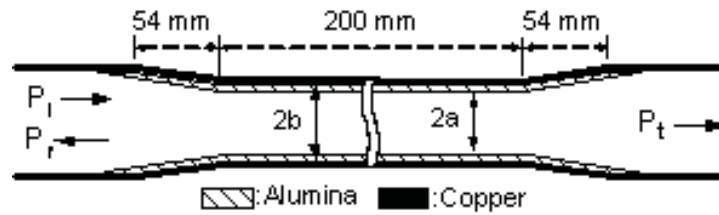


**FIGURE 1.** Cross section of the cylindrical alumina DLA structure ( $a = 5$  mm;  $b = 7.185$  mm). Structure is shown with the tapered matching sections (54 mm) and central accelerating section (200 mm).

Since this initial report, single-surface multipactor has been observed in all DLA structures tested at high power. These structures have been fabricated from a variety of materials, some with low-secondary-emission surface coatings, and with different physical dimensions, and new phenomena have been observed. In this paper, we summarize the results of high-power tests of DLA structures fabricated from alumina, TiN-coated alumina, magnesium calcium titanate (MCT) and fused silica (quartz), and analyze the results in terms of a physical model of the multipactor phenomenon. An accompanying paper provides a closer look at data from the quartz structure [3].

## EXPERIMENTAL SETUP

The configuration used during the high power tests is shown in Fig. 2. The magnicon (not shown) output is delivered through WR-90 vacuum waveguide, equipped with two 55.5 dB bi-directional coupler connected to calibrated crystal detectors, and into the input coupler of the DLA structure. The output of the DLA structure is delivered through a short section of WR-90 equipped with an identical bi-directional coupler and into a SLAC-type high-power load. The diagnostics available to monitor the DLA structure during high power conditioning included (1) directional couplers on both the input and output waveguide to monitor the incident, reflected, and transmitted power; (2) four ion pumps to maintain the vacuum and monitor the pressure; (3) a Faraday cup downstream of the structure to monitor dark current; and (4) cameras to look for visible light along the axis of the structure in the event of a breakdown.

## SUMMARY OF EXPERIMENTAL RESULTS

Single-surface multipactor has been observed in all the DLA structures that have undergone high power testing. We have now tested four types of structures fabricated from a variety of materials, some with low secondary-emission surface coatings, and having different physical dimensions, and new phenomena have been observed. In Table I, we summarize the results of high-power tests of the four DLA structures tested to date. These include the alumina ( $\text{Al}_2\text{O}_3$ ), TiN-coated alumina ( $\text{Al}_2\text{O}_3$ ), magnesium calcium titanate or MCT ( $\text{Mg}_x\text{Ca}_{1-x}\text{TiO}_3$ ) and fused silica ( $\text{SiO}_2$ ) DLA structures.

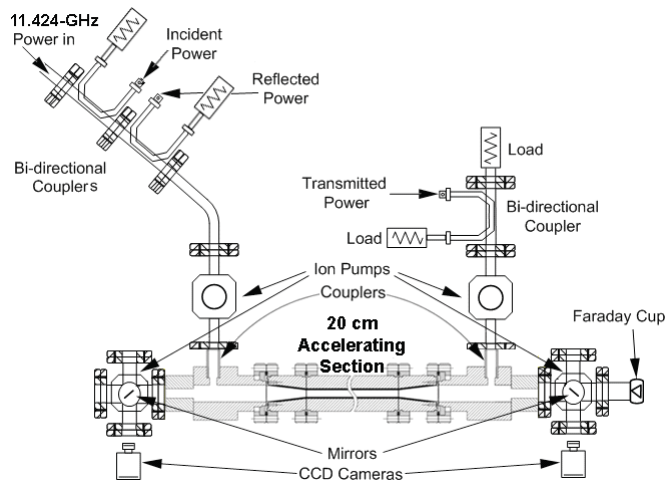


FIGURE 2. Experimental setup used during high-power tests at NRL.

While multipactor has been observed in all four types of structures tested, each structure displays certain unique features. In Fig. 3, we show the normalized fraction of transmitted power ( $S_{21}$ ) for ease of comparison, since the absolute value of  $S_{21}$  between the structures varies due to the quality of the assembly, the loss tangent of the ceramic, and the ohmic loss at the metal surface outside the ceramic. We also show the same data plotted with both a logarithmic (Fig. 3a) and a linear (Fig. 3b) scale to emphasize the low power and high power behavior respectively.

All four structures demonstrate similar low power behavior (see Fig. 3a); e.g., there is no multipactor-induced drop in  $S_{21}$  until a threshold is crossed. However, once the incident power is raised above that threshold, the high power behavior (see Fig. 3b) varies considerably. The non-coated Alumina DLA structure exhibits the most severe multipactor-induced power loss in both its magnitude and in the fact that  $S_{21}$  is continuing to drop even at the highest power tested. The TiN-coated Alumina and the Fused Silica structures level off at high incident power, indicating a reduced multipactor effect. Lastly, the MCT-20 DLA structure has the weakest multipactor effect but was tested at the lowest power due to rf breakdown at a ceramic joint where the local field was on the order of 100 MV/m.

TABLE 1. Summary of the structure parameters and key experimental results of the DLA structures that have been tested at high power to date

Material	$\text{Al}_2\text{O}_3$ †	$\text{Mg}_x\text{Ca}_{1-x}\text{TiO}_3$	$\text{SiO}_2$
Dielectric constant	9.4	20	3.78
Loss tangent	$2 \times 10^{-4}$	$3 \times 10^{-4}$	$2 \times 10^{-5}$
Inner radius	5 mm	3 mm	8.971 mm
Outer radius	7.185 mm	4.567 mm	12.079 mm
R/Q	6.9 k $\Omega$ /m	8.8 k $\Omega$ /m	3.6 k $\Omega$ /m
Group velocity	$0.134c$	$0.057c$	$0.38c$
RF power for 1MV/m gradient	80 kW	27 kW	439 kW
Demonstrated Gradient	8 MV/m	7.2 MV/m	5 MV/m
Principal Problem	Multipactor	Breakdown at joints	Multipactor

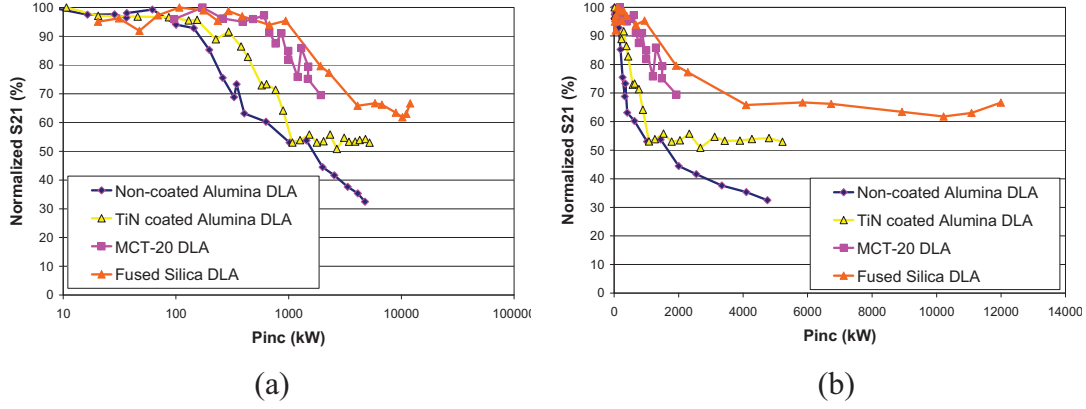


**FIGURE 3.** Comparison of multipactor-induced RF loading for the four DLA structures that have undergone high-power testing shown on (a) a log plot and (b) a linear plot.

There are several possible explanations as to why the four structures differ in their multipactor-induced power loss. These include differences in the SEE properties of the materials, differences in permittivity, and differences in the geometry of the tube. In the following sections, we develop and apply a 1D theory to explain these differences.

## 1D THEORY

In this section, we briefly summarize the 2D numerical model that was given in Ref. [1] that was used to model the saturation condition and then show how we can explain the same phenomena with a simpler 1D analytic theory. The 2D model essentially consists of three parts: (1) A model of the secondary electron emission (SEE) properties of the material that includes five parameters:  $e_0$ ,  $e_1$ ,  $e_2$ ,  $K$ , and  $\delta$ . SEE multiplication can occur when a primary electron gains energy from the rf field and strikes the surface with an impact energy  $K$  in the energy band between  $e_1$  and  $e_2$ , where the secondary electron yield  $\delta$  (the ratio of electrons emitted from the surface to electrons impacting the surface) is greater than 1 [4]. On average,  $\delta$  secondaries per primary are emitted from the surface with emission energy  $e_0$ . (2) Expressions for the  $TM_{01}$  fields in the vacuum region of the DLA structure:

$$E_z = E_{z0} I_0(k_r r) \cos(\omega t - k_z z) \quad (1)$$

$$E_r = E_{z0} \left( \frac{k_z}{k_r} \right) I_1(k_r r) \sin(\omega t - k_z z) \quad (2)$$

where  $E_{z0}$  is the rf field amplitude,  $k_r$  and  $k_z$  are the radial and longitudinal wave numbers, respectively,  $\omega$  is the angular frequency, and  $I_n(x)$  is the modified Bessel function of the first kind. (3) A DC space charge field ( $E_{DC}$ ) to represent the electric field of the secondaries near the surface. Given these 3 components of the model, the equations of motion can be integrated to obtain the electron trajectories using the initial condition that the emission velocity is given by  $v_0 = \sqrt{2e_0/m}$ .

$$m\ddot{z} = -eE_{z0} \cos(\omega t - k_z z + \theta) \quad (3)$$

$$m\dot{r} = -eE_{DC} - eE_{z0} \left( \frac{\pi a}{\lambda_z} \right) \sin(\omega t - k_z z + \theta) \quad (4)$$

The multipactor-induced power loss ( $P_m$ ) can be calculated as

$$P_m = N_e K / \tau \quad (5)$$

where  $N_e$  is the number of electrons in the structure with impact energy  $K$  striking the surface per hop time  $\tau$ . Saturation occurs when the emission of the secondaries is suppressed due to the build up of the space charge cloud given by

$$eN_e = 2\pi a \epsilon_0 E_{DC} L. \quad (6)$$

Using results from the 2D numerical model, we now develop a 1D theory. We make use of two observations from the 2D model: (i) multipactor is dominated by  $E_r$  and we can therefore ignore the  $z$  motion, thus simplifying the equation of motion to

$$m\dot{r} = -eE_{DC} - eE_{z0} \left( \frac{\pi a}{\lambda_z} \right) \sin(\omega t + \theta), \quad (7)$$

and (ii) the multipactor is resonant and the electron hop along the surface at  $\tau = T_{rf}$ .

We now derive an analytic expression for Eq. (5). Since we already have  $\tau = T_{rf}$ , this only requires analytic expressions for  $N_e$  and  $K$ . Solving Eq. (7) for  $r(t)$ , we can make use of the fact that, at saturation, the resonant electron takes exactly one RF period to return to the surface and set  $r(\tau = T_{rf}) = 0$ . From this we can solve for the space charge field needed to return the particle to the surface,

$$E_{DC} = \frac{m\omega}{e\pi} - E_{z0} \left( \frac{a}{\lambda_z} \right) \cos(\theta) \quad (8)$$

At saturation, we are interested in the last available phase at which a trajectory resonates, so we set  $\theta = \pi$  in Eq. (8). Next, we solve Eq. (7) for the impact velocity and now have an expression for the impact energy at  $\tau = T_{rf}$ ,

$$K = \frac{1}{2} m v_r^2 = \frac{1}{2} m \left( v_0 - \frac{e T_{rf}}{m} E_{DC} \right)^2. \quad (9)$$

Substitution of Equations (8) and (9) into (6) yield an analytic prediction of the multipactor-induced power loss.

Before moving to the comparison of the 1D theory to the experimental results, we give the 1D theory predictions of  $P_m$  scaling with  $E_r$ :

$$P_m \propto E_r^3. \quad (10)$$

## COMPARISON OF THEORY TO EXPERIMENT

In order to compare the four DLA structures to the theory, we first correct for four factors: (1) Since the tubes are of different lengths, we compare the power loss on a

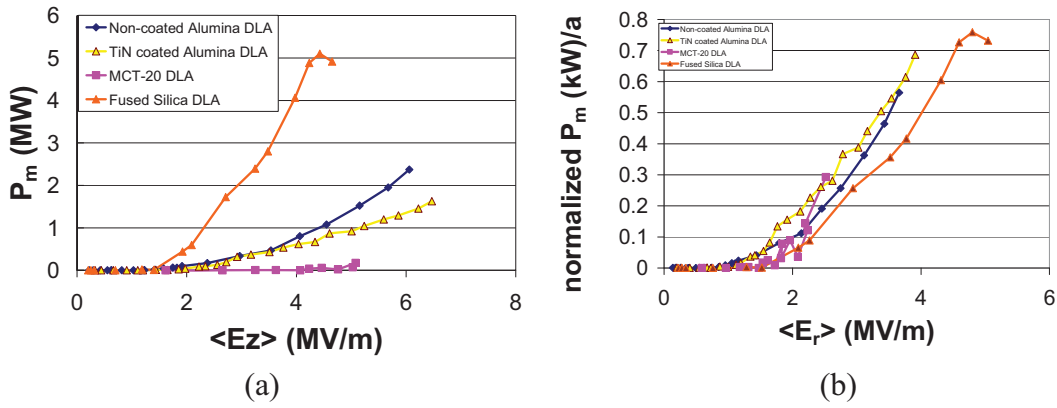


**FIGURE 4.** Comparison of multipactor-induced RF loading for the four DLA structures. Data has been corrected for length and shunt impedance. (a)  $P_m$  vs.  $E_z$  and (b)  $P_m$  vs  $E_r$ .

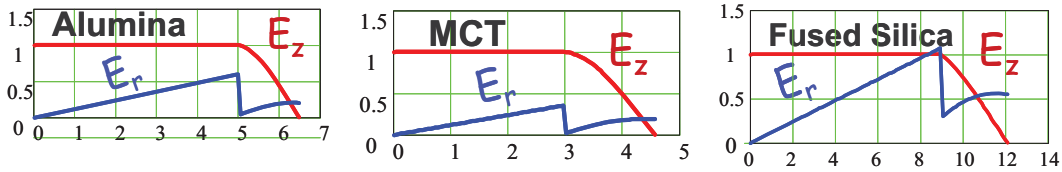


**FIGURE 5.** Relative value of the TM<sub>01</sub> electric field vectors in the vacuum and dielectric regions.

per-unit-length basis. (2) Since each tube has a different shunt impedance (i.e. requires a different incident RF power for 1MV/m gradient, see Table 1.), we compare the structures on the basis of  $E_z$  in Fig. 4. (3) Next, given the strong scaling of  $P_m$  with  $E_r$  (see Eq. (10)), we expect that structures with larger radial electric field at the surface,  $E_r(r=a)$ , to have larger multipactor. In Fig. 5, we plot the relative value of the TM<sub>01</sub> electric field vectors in the vacuum region. In particular, the ratio of  $E_r/E_z = \pi a/\lambda_z = 0.6$  (alumina), 0.36 (MCT), and 1.08 (fused silica) at the inner surface of the dielectric  $r=a$ . From this we see why the multipactor effect was largest in fused silica and smallest in MCT. (4) Lastly, from Eq. (6),  $N \propto a$ . From this and Eq. (10), we can predict the scaling of  $P_m$  with  $a$ ,

$$P_m \propto a^4. \quad (11)$$

All four of these factors are accounted for in Fig. 4b, where  $P_m/a$  is plotted against  $E_r$ . Notice that once these geometrical factors are taken into account, the multipactor behavior of the four DLA structures has only minor differences, thus indicating that the differences observed during the high-power tests are mostly due to geometrical differences in the structures.

Finally, we compare the 1D theory directly to the data in Fig. 6. The theory shown in Fig. 6 has been arbitrarily scaled upward by 25% to improve the quantitative agreement. The agreement of the simple 1D theory and the experiment is relatively good, with the inclusion of this scaling factor, except for fused silica, where the theory overestimates the observed data. Since all geometrical factors have been accounted for, this means that the disagreement for fused silica must be due to SEE material

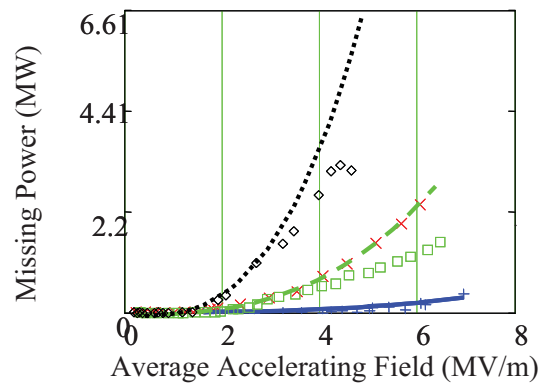


**FIGURE 6.** Comparison of the 1D theory to the experiment. Fused Silica data = diamonds; Alumina data = X; TiN-coated alumina =squares; MCT-20 data=plus; Fused Silica theory = top line; Alumina theory = middle line; MCT-20 theory = bottom line.

difference. Indeed, if the emission energy  $e_0$  is lowered from the values used for the others structures ( $e_0=2\text{eV}$ ) to  $e_0=0.1\text{ eV}$ , the agreement (not shown) is excellent.

## FUTURE DIRECTIONS

The most important question for the future of the DLA structure is what happens at higher power. Since multipactor in the DLA structure is a resonant process, it is reasonable to expect that we can hop over the multipactor regime. This would happen because the high RF fields would accelerate the secondaries to impact energies above the second crossover energy,  $e_2$ , where no multipactor is possible. Also, it is possible that if the risetime of the RF pulse is very short (e.g. in a dielectric wakefield accelerator), there will not be sufficient time for the multipactor to avalanche to saturation.

To address these issues, we plan to extend the theory and numerical model to investigate scaling with length ( $L$ ), frequency ( $f$ ), and RF pulse length ( $\Delta\tau$ ), and to include the second cross-over energy ( $e_2$ ) and  $\delta$ , as well as a realistic emission distribution ( $e_0$ ). One important feature in the data that was not explained in this paper is why the multipactor-induced power loss levels off at high power for fused silica and the TiN-coated alumina structure. Preliminary modeling indicates that this is due to a change in the emission energy ( $e_0$ ) of the material. In addition to the theory and modeling, we will also continue to test the multipactor scaling laws experimentally, in the course of the high-power testing program that is currently under way.

## ACKNOWLEDGMENTS

This work was supported by the Division of High Energy Physics, U.S. Department of Energy and by the US Office of Naval Research.

## REFERENCES

1. J. G. Power et al., *Phys. Rev. Lett*, **92**, 164801, 23 April 2004.
2. S. H. Gold et al., paper in this Proceedings.
3. C. Jing et al., paper in this Proceedings.
4. J. R. M. Vaughn, *IEEE Trans. Electron Devices* **36**, 1963 (1989).